Conductive F-doped Tin Dioxide Sol−Gel Materials from Fluorinated β-Diketonate Tin(IV) Complexes. Characterization and Thermolytic Behavior

Angélina Gamard,[†,‡] Odile Babot,[†] Bernard Jousseaume,[†] Marie-Claude Rascle,[†] Thierry Toupance,*[,†] and Guy Campet[‡]

Laboratoire de Chimie Organique et Organométallique, UMR 5802 CNRS, Université Bordeaux I, 351 Cours de la Libération, F33405 Talence Cedex, France, and Institut de Chimie de la Matière Condensée de Bordeaux, UPR 9048 CNRS, Château Brivazac, Avenue du Docteur A. Schweitzer, F33608 Pessac Cedex, France

Received April 27, 2000. Revised Manuscript Received July 31, 2000

Hydrolysis and condensation of $(CH_3COCHCOCH_3)_2SnF(O\textit{tert}\text{-Am})$ and $(CF_3COCHCOCH_3)_2Sn(O\textit{tert}\text{-Am})_2$ gave soluble stannic oxo-oligomers or -polymers including fluorine and β-diketonate groups. Under thermal treatment in air at 550 °C, they yielded nanocrystalline fluorine-doped tin dioxide powders. The amount of remaining ligands in the xerosols depends on the hydrolysis ratio and on the nature of the solvent used, dimethylformamide (DMF) favoring ligand removal. The thermolytic reactions have been investigated by thermogravimetry coupled to mass spectrometry: (1) the β-diketonate ligands pyrolyze in two stages, at 200 and 320 °C, involving two different processes; (2) elimination of polar solvents of high boiling point, such as DMF, occurs up to 300 °C; (3) fluorine is lost as fluorhydric acid from 230 °C. The best strategy to prepare F-doped SnO_2 materials by the sol−gel route is thus to start from precursors including Sn−F bonds and to use a polar aprotic solvent of low boiling point such as acetonitrile. It led to nanocrystalline, highly conductive F-doped tin dioxide materials with resistivities 1 order of magnitude lower than that reported for Sb-doped tin dioxide powders.

Introduction

Applications of undoped or doped tin dioxide thin films and colloids are numerous because of their high mechanical, chemical, and environmental stabilities, even at high temperature, and their remarkable optical and electrical properties.[1] They include transparent conductive electrodes,[2] photovoltaic devices,[3] catalysis,[4] gas sensors,[5] antistatic coatings,[6] and preparation of conductive layers.[7] To obtain such materials, techniques such as r.f. magnetron sputtering,[8] spray pyrolysis,[9] and chemical vapor deposition (CVD)[10] were preferred to reach dense and highly conductive coatings, whereas porous and nanocrystalline materials were generally obtained by hydrolytic processes including sol−gel.[11]

Reports dealing with undoped and antimony-doped tin dioxide colloïds,[12] nanoparticles,[13] and sol−gel films[14] have been described. However, very few works have been devoted to the sol−gel preparation of similar

* To whom correspondence should be addressed. E-mail: t.toupance@lcoo.u-bordeaux.fr.

† UMR 5802.

‡ UPR 9048.

(1) Chopra, K. L.; Major, S.; Pandya, D. K. *Thin Solid Films* **1983**, *102*, 1.

(2) (a) Cachet, H.; Bruneaux, J.; Folcher, G.; Lévy-Clément, C.; Vard, C.; Neumann-Spallart, M. *Sol. Energy Mater. Sol. Cells* **1997**, *46*, 101. (b) Andersson, A.; Johansson, N.; Bröms, P.; Yu, N.; Salaneck, W. R. *Adv. Mater.* **1998**, *10*, 859.

(3) (a) Bedja, T.; Hotchandani, S.; Kamat, P. V. *J. Phys. Chem.* **1994**, *98*, 4133. (b) Ferrere, S.; Zaban, A.; Gregg, B. A. *J. Phys. Chem. B* **1997**, *101*, 4490. (c) Ford, W. E.; Wessls, J. M.; Rodgers, M. A. J. *J. Phys. Chem. B* **1997**, *101*, 7435.

(4) Cebolla, V. C.; Bacaud, R.; Besson, M.; Cagniant, D.; Charcosset, H.; Oberson, M. *Bull. Soc. Chim. Fr.* **1987**, 935.

(5) (a) Harrison, P. G.; Willett, M. J. *Nature* **1988**, *332*, 337. (b) Sberveglieri, G. *Sensors Actuators B* **1992**, *6*, 239. (c) Diéguez, A.; Romano-Rodriguez, A.; Morante, J. R.; Weimar, U.; Schweizer-Berberich, M.; Göpel, W. *Sensors Actuators B* **1996**, *31*, 1. (d) Rella, R.; Serra, A.; Siciliano, P.; Vasanelli, L.; De, G.; Licciulli, A. *Thin Solid Films* **1997**, *304*, 339.

(6) (a) Sonoda, N.; Shimotsuma, W.; Tsubusaki, S. U.S. Patent 4246143, 1981. (b) Robert, J. C. U.S. Patent 5494652, 1996.

(7) (a) Goebbert, C.; Aegerter, M. A.; Burgard, D.; Nass, R.; Schmidt, H. *J. Mater. Chem.* **1999**, *9*, 253. (b) Cao, L.; Huo, L.; Ping, G.; Wang, D.; Zeng, G., Xi, S. *Thin Solid Films* **1999**, *247*, 258. (c) Goebbert, C.; Nonninger, R.; Aegerter, M. A.; Schmidt, H. *Thin Solid Films* **1999**, *351*, 79.

(8) Geoffroy, C.; Campet, G.; Menil, F.; Portier, J.; Salardenne, J.; Couturier, G. *Active Passive Elec. Comput.* **1991**, *14*, 111.

(9) (a) Smith, A.; Laurent, J. M.; Smith, D. S.; Bonnet, J. P.; Clemente, R. R. *Thin Solid Films* **1995**, *266*, 20. (b) Morris, G. C.; McElnea, A. E. *Appl. Surf. Sci.* **1996**, *92*, 167. (c) Park, S. H.; Son, Y. C.; Willis, W. S.; Suib, S. L.; Creasy, K. E. *Chem. Mater.* **1998**, *10*, 2389. (d) Shanthi, S.; Subramanian, C.; Ramasamy, P. *Mater. Sci. Eng.* **1999**, *B57*, 127.

(10) (a) Maruyama, T.; Tabata, K. *J. Appl. Phys.* **1990**, *68*, 4282. (b) Proscia, J.; Gordon, R. G. *Thin Solid Films* **1992**, *214*, 175. (c) Suh, S.; Hoffmann, D. M.; Atagi, L. M.; Smith, D. C.; Liu, J.-R.; Chu, W.-K. *Chem. Mater.* **1997**, *9*, 730. (d) Suh, S.; Zhang, Z.; Chu, W.-K.; Hoffman, D. M. *Thin Solid Films* **1999**, *345*, 240.

(11) Ocana, M.; Matijevic, E. *J. Mater. Res.* **1990**, *5*, 1083.

(12) (a) Ocana, M.; Serna, C. J.; Matijevic, E. *Colloid Polym. Sci.* **1995**, *273*, 681. (b) Nutz, T.; Felde, U.; Haase, M. *J. Phys. Chem. B* **1999**, *110*, 12142.

(13) Nayral, C.; Ould-Ely, T.; Maisonnat, A.; Chaudret, B.; Fau, P.; Lescouzères, L.; Peyre-Lavigne, A. *Adv. Mater.* **1999**, *11*, 61.

(14) (a) Terrier, C.; Chatelon, J. P.; Berjoan, R.; Roger, J. A. *Thin Solid Films* **1995**, *263*, 37. (b) Chatelon, J. P.; Terrier, C.; Roger, J. A. *J. Sol-Gel Sci. Technol.* **1997**, *10*, 55. (c) Aegerter, M. A.; Reich, A.; Ganz, D.; Gasparro, G.; Pütz, J.; Krajewski, T. *J. Non-Cryst. Solids* **1997**, *218*, 123. (d) Gasparro, G.; Pütz, J.; Ganz, D.; Aegerter, M. A. *Sol. Energy Mater. Sol. Cells* **1998**, *54*, 287.

10.1021/cm001073k CCC: $19.00
Published on Web 10/21/2000

Scheme 1. Schematic Representation of the Sol−Gel Precursors Used in This Study {(1) *tert*-Amyloxyfluoro(dipentan-2,4-dionato)tin(IV); (2) Bis(*tert*-amyloxy)bis(1,1,1-trifluoropentan-2,4-dionato)tin(IV); (3) Bis(*tert*-amyloxy)(dipentan-2,4-dionato)tin(IV)}

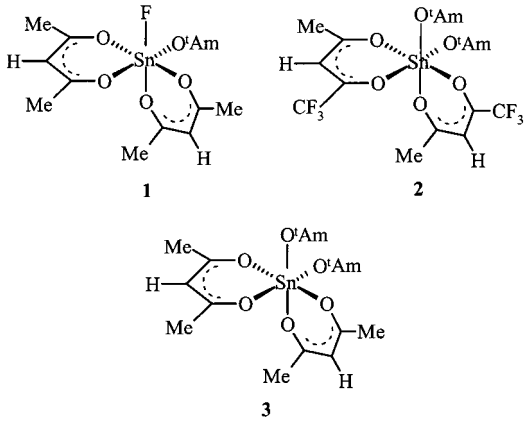

F-doped materials,[15] although fluorine is the most efficient doping agent to reach the highest electronic conductivity and IR reflectivity.[1] In addition, the wide range of viscosity attainable by the sol−gel process permits processing of fibers, coatings, or powders, and subsequent thermal treatment, including both drying and densification steps, yields the desired materials.[16] To break into that field, we designed new unimolecular precursors, alkoxyfluoro(dipentan-2,4-dionato)tin(IV) complexes **1** (Scheme 1), in which each chemical bond desired in the final material was already present.[17] They furnished soluble fluorous stannic oxopolymers upon hydrolysis,[17a] which gave, after thermal treatment, the first conductive F-doped SnO_2 materials prepared by the sol−gel route. Nevertheless, it was of basic importance to point out precisely the factors that govern the nature of the xerosols and their conductivity properties after thermolysis.

The aim of this work was to have a better view of the influence of the hydrolysis parameters (choice and concentration of the precursor, solvent nature, initial hydrolysis ratio $h = [H_2O]/[M]$) on the nature of the xerosols and to study their decomposition process during thermal treatment. The relevance of the pre-existence of a Sn−F bond in the precursor so as to obtain low resistivities is also emphasized by comparison with materials prepared from molecules **2** and **3** (Scheme 1) where the fluorine atoms are either located on ligands or are not present, respectively.

Experimental Section

Materials. Reactants and products were handled under a nitrogen atmosphere by using standard Schlenk techniques. All the solvents used were distilled prior to use: acetonitrile, dimethylformamide (DMF) over CaH_2, and *n*-hexane from sodium benzophenone ketyl. Solution NMR and mass analyses were carried out on spectrometers previously described.[17a] Infrared spectra (KBr pellets) were recorded in the absorption mode using a FTIR Perkin-Elmer spectrophotometer. Elemental analyses were performed in the Center of Chemical Analysis of the "Centre National de la Recherche Scientifique" (Vernaison, France). The water content was determined by the classical Karl−Fischer method with short contact time to avoid the titration of surface hydroxyl functions.

Fluoro(*tert*-amyloxy)di(pentan-2,4-dionato)tin(IV) **1**[17a] and bis(*tert*-amyloxy)di(pentan-2,4-dionato)tin(IV) **3**[18] complexes were synthesized as previously reported.

Bis(*tert*-amyloxy)di(1,1,1-trifluoropentan-2,4-dionato)tin-(IV) **2** was obtained from tetra(*tert*-amyloxy)tin(IV) and 1,1,1-trifluoropentan-2,4-dione (Acros Organics).[19] Compound **2** probably exists in solution as a mixture of three cis forms.[20]

Preparation of the Xerosols. Hydrolysis experiments were performed as follows in two solvents of different polarity, acetonitrile and dimethylformamide. To a stirred solution of precursor in the chosen solvent was added slowly a mixture of water and solvent. The molar ratio between solvent and precursor was maintained around 50:1 and the hydrolysis ratio $h = [H_2O]/[\text{precursor}]$ was increased from 0.5 to 10. After the mixture was stirred for 1 h at room temperature, sols, gels, or precipitates were obtained, depending on the solvent nature and the *h* value. For both precursors, sols were obtained in acetonitrile for $h < 3$ and in DMF for $h \leq 10$. The solvent and volatile compounds were removed under vacuo at 50 °C to yield white or yellow powders, which were then washed several times with *n*-hexane. Subsequently, drying under vacuum at 70 °C yielded the xerosols. The as-prepared materials could be redissolved in the parent solvent, permitting ^{19}F and ^{119}Sn NMR spectroscopy analyses. The characterizations of four xerosols, labeled X_2^A (**1**, $h = 2$, CH_3CN), X_2^D (**1**, $h = 2$, DMF), X_{10}^D (**1**, $h = 10$, DMF), and Y_2^A (**2**, $h = 2$, CH_3CN), are emphasized in this paper:

(X_2^A) **1**: 6.73 g, 15.9 mmol. H_2O: 0.58 g, 32.2 mmol. CH_3CN: 39.4 mL. After drying, 3.78 g of a yellow powder was recovered. Elemental analysis. Calculated for $SnFO_{1.05}(C_5H_7O_2)_{0.9}\cdot 0.72H_2O$: wt % Sn = 46.26, wt % F = 7.40, wt % C = 21.06, wt % H = 3.04, wt % H_2O = 5.05. Found: wt % Sn = 45.94, wt % F = 7.30, wt % C = 20.81, wt % H = 2.94, wt % H_2O = 5.01.

(X_2^D) **1**: 4.79 g, 11.3 mmol. H_2O: 0.43 g, 23.6 mmol. DMF: 43.6 mL. After drying, 1.97 g of a yellow powder was recovered. Elemental analysis. Calculated for $SnFO_{1.27}(C_5H_7O_2)_{0.46}(DMF)_{0.7}\cdot 0.67H_2O$: wt % Sn = 48.90, wt % F = 7.82, wt % C = 16.87, wt % H = 2.97, wt % N = 2.13, wt % H_2O = 4.97. Found: wt % Sn = 49.16, wt % F = 7.83, wt % C = 16.98, wt % H = 2.99, wt % N = 2.14, wt % H_2O = 5.02.

(X_{10}^D) **1**: 8.32 g, 19.7 mmol. H_2O: 3.55 g, 197 mmol. DMF: 75.7 mL. After drying, 4.74 g of a yellow powder was recovered. Elemental analysis. Calculated for $SnFO_{1.47}(C_5H_7O_2)_{0.07}(DMF)_{0.83}\cdot 1.9H_2O$: wt % Sn = 45.12, wt % F = 7.22, wt % C = 12.96, wt % H = 3.87, wt % N = 4.41, wt % H_2O = 13. Found: wt % Sn = 44.85, wt % F = 7.19, wt % C = 12.91, wt % H = 3.35, wt % N = 4.39, wt % H_2O = 12.5.

(Y_2^A) **2**: 3.05 g, 5.1 mmol. H_2O: 0.19 g, 10.5 mmol. CH_3CN: 12.3 mL. After drying, 1.88 g of a yellow powder was recovered. Elemental analysis. Calculated for $SnO_{1.4}(C_5H_4F_3O_2)_{1.2}\cdot 0.9H_2O$: wt % Sn = 34.80, wt % F = 20.05, wt % C = 21.13, wt % H = 1.95, wt % H_2O = 4.75. Found: wt % Sn = 34.13, wt % F = 20.23, wt % C = 19.81, wt % H = 2.23, wt % H_2O = 4.58.

For comparison, complex **3** was also hydrolyzed for $h = 2$ in acetonitrile. The resulting xerosol (Z_2^A) was previously described by Armelao et al.[18]

(15) Ray, S. C.; Karanjai, M. K.; DasGupta, D. *Surf. Coat. Technol.* **1998**, *102*, 73.

(16) (a) Brinker, C. J.; Scherer, G. W. *Sol−Gel Science*; Academic Press: San Diego, 1990. (b) Hench, L. L.; West, J. K. *Chem. Rev.* **1990**, *90*, 33.

(17) (a) Gamard, A.; Jousseaume, B.; Toupance, T.; Campet, G. *Inorg. Chem.* **1999**, *38*, 4671. (b) Gamard, A. Ph.D. Thesis, University Bordeaux I, 1999. (c) Boegeat, D.; Jousseaume, B.; Toupance, T.; Campet, G.; Fournès, L. *Inorg. Chem.* **2000**, *39*, 3924.

(18) Armelao, L.; Ribot, F. O.; Sanchez, C. *Better Ceramic Through Chemistry VII: Organic Inorganic Hybrid Materials*; Coltrain, B., Sanchez, C., Schaefer, D. W., Wilkes, G. L., Eds.; Materials Research Society, Pittsburgh, PA, 1996; p 387.

(19) See Supporting Information.

(20) See Supporting Information. Also, see Chandler, C. D.; Fallon, G. D.; Koplick, A. J.; West, B. O. *Aust. J. Chem.* **1987**, *40*, 1427.

Pyrolysis Experiments and Characterization of the Products. Thermal analyses were carried out on a Netzsch STA simultaneous analyzer. Thermogrametry (TG) and derivative thermogravimetry (DTG) analyses were recorded in the range 50−650 °C under helium or argon flow at a heating rate of 10 °C min^{-1}. Mass analyses were performed on a Thermostar Balzers Instruments quadrupole spectrometer. Powder samples were placed in alumina crucibles. Electron impact mass spectra (70 eV) were continuously recorded and stored, with scans from 3 to 300 amu. Each scan was recorded in 0.5 s with a delay time of 0.1 s. Thermolysis was performed by treating xerosols in air for 30 min at 550 °C. The chemical composition of the resulting powders was determined by elemental analysis:

xerosol: X_2^A; (exptl) wt % Sn = 76.95, wt % F = 0.79, wt % C = 0.93

xerosol: X_2^D; (exptl) wt % Sn = 75.18, wt % F = 0.96, wt % C = 1.21

xerosol: X_{10}^D; (exptl) wt % Sn = 73.20, wt % F = 0.94, wt % C = 1.18

xerosol: Y_2^A; (exptl) wt % Sn = 76.75, wt % F = 0.51, wt % C = 0.69

xerosol: Z_2^A; (exptl) wt % Sn = 75.94, wt % C = 0.84

The Mössbauer resonance spectra were obtained with a constant acceleration Halder-type spectrometer with a room-temperature $CaSnO_3$ source in a transmission geometry. The spectra were fitted to the sum of Lorentzians by least-squares refinements. All isomeric shifts given in the communication refer to $CaSnO_3$ at 293 K. Crystallinity of the materials was checked by powder X-ray diffraction using a Philips $\theta-2\theta$ PW1820 diffractometer. The average particle size was deduced from the half-height line broadening by applying the Laue−Scherrer formula assuming Gaussian profiles for experimental and instrumental broadening.[21] The sample resistivity was estimated by compacting under pressure (10 ton) a given amount of powder (200 mg) between two stainless steel cylinders. The resistance R_s of the pelletized materials (13-mm diameter, 0.40-mm thickness) was measured with a Rhopoint M210 Milli-ohmeter. The measurements were performed under pressure (0.5 ton) using the previous cylinders as contacts. The sample resistivity ρ_s was deduced from R_s by the simple formula $\rho_s = SR_s/e$, where S and e are the surface and the thickness of the sample, respectively.

Results and Discussion

Tin tetraalkoxides generally lead to precipitates in the presence of water.[22] As already proposed for other metals,[23] a ligand exchange with β-diketones allows the tin tetraalkoxides to modify their reactivity toward hydrolysis and condensation. Sanchez et al. indeed showed that the hydrolysis of **3** gave stable sols when polar and coordinating solvents were used.[18] The same strategy was used in this study for **1** and **2**. Acetonitrile and dimethylformamide (DMF) were investigated as solvents to perform hydrolysis experiments. Qualitative results for different hydrolysis ratios h are listed in Table 1. Precursors **1** and **2** behaved roughly similar to **3** and yielded stable sols for h up to 2 in CH_3CN and up to 10 in DMF. By evaporation of the solvent, these sols gave xerosols, soluble in the parent solvent. To keep a sufficient fluorine amount in the xerosols, we focused on four xerosols, labeled X_2^A (**1**, $h = 2$, CH_3CN), X_2^D (**1**, $h = 2$, DMF), X_{10}^D (**1**, $h = 10$, DMF), and Y_2^A (**2**, $h = 2$, CH_3CN).

Table 1. Hydrolytic Behavior of Complexes 1 and 2 (S, sol; G, gel; P, precipitate)

precursor	solvent	$h = 1$	$h = 2$	$h = 3$	$h = 10$
1	CH_3CN	S	S	G	G
1	DMF	S	S	S	S
2	CH_3CN	S	S	G	P

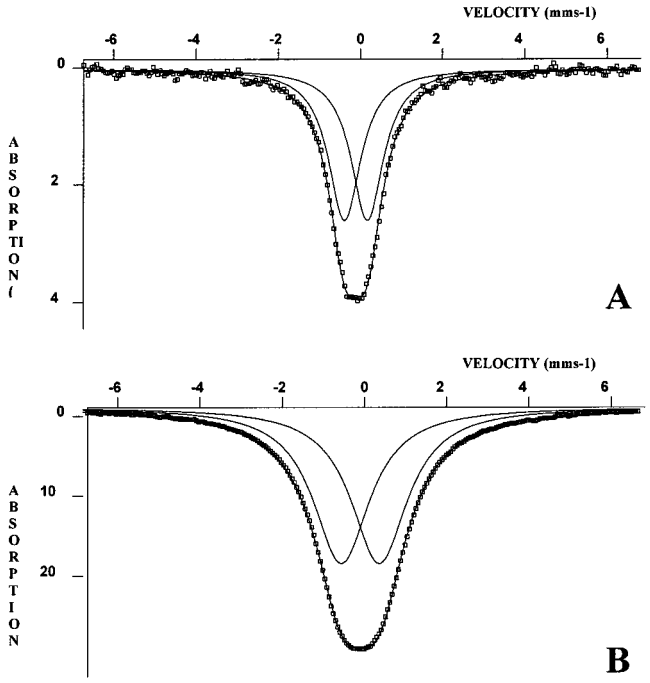

Figure 1. Room-temperature experimental and fitted Mössbauer spectra recorded for xerosol X_2^A after (A) drying and (B) treatment in air at 550 °C for 30 min.

Characterization of the Xerosols. Preliminary studies carried out on xerosol X_2^A showed that it probably contained stannic fluorinated oxo-oligomeric or -polymeric species bearing β-diketonate ligands.[17a] To assess its structure, further investigations were conducted. The room-temperature Mössbauer spectrum of X_2^A (Figure 1A) exhibited a broad single band assigned to a distorted tin(IV) site having an isomeric shift $\delta = -0.08$ mm s^{-1} and a quadrupolar splitting $\Delta = 0.56$ mm s^{-1}. On the basis of the isomeric shifts reported for SnO_2 ($\delta = 0$ mm s^{-1}) and SnF_4 ($\delta = -0.36$ mm s^{-1}),[24] the slightly negative value found for δ confirms the presence of a fluorine atom on the tin. In addition, the rather large quadrupolar splitting Δ observed was consistent with the chemical variety of groups present in the neighborhood of the tin center. The IR spectrum of xerosol X_2^A (Figure 2) clearly shows bands due to

(21) The mean particle size is given by the Laue-Scherrer relation $t = (\lambda/\epsilon \cos\theta)$, with $\epsilon = (\epsilon_m^2 - \epsilon_0^2)^{1/2}$, where θ is the Bragg angle for the chosen hkl reflection and ϵ_m and ϵ_0 are, the angular half-widths of the hkl peak for the studied sample and well-crystallized SnO_2 without size effect, respectively. See Eberhardt, J. P. *Structural and Chemical Analysis of Materials*; John-Wiley & Sons: New York, 1991, 203.

(22) Giuntini, J. C.; Granier, W.; Zanchetta, J. V.; Taha, A. *J. Mater. Sci. Lett.* **1990**, *9*, 1383.

(23) Sanchez, C.; Livage, J.; Henry, M.; Babonneau, F. *J. Non-Cryst. Solids* **1988**, *100*, 65.

(24) Fournès, L.; Grannec, J.; Potin, Y.; Hagenmuller, P. *Solid State Commun.* **1986**, *59*, 833.

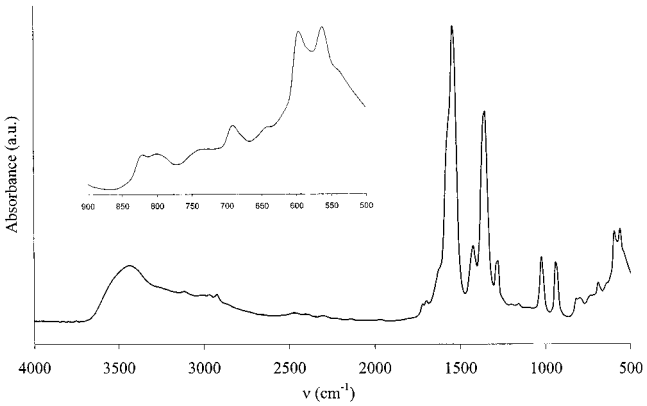

Figure 2. FTIR spectra of xerosol X_2^A after drying. The 900−500-cm^{-1} region of the dried X_2^A spectrum is shown in the inset.

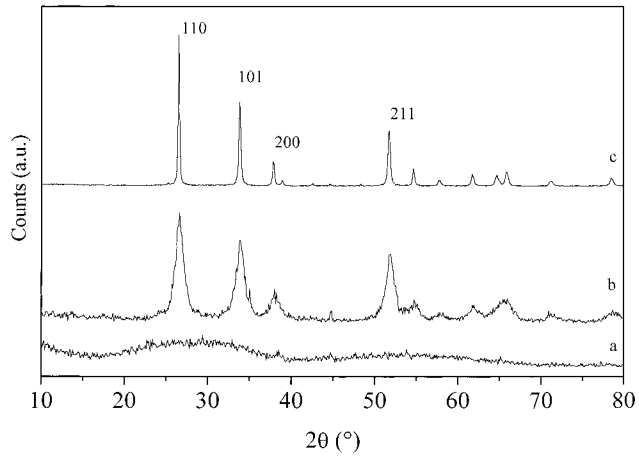

Figure 3. X-ray diffraction pattern of (a) xerosol X_2^A after treament in air at 60 °C for 3 days, (b) xerosol X_2^A after treament in air at 550 °C for 30 min, and (c) commercial tin dioxide after treament in air at 550 °C for 30 min.

acetylacetonato ligands coordinated to tin at 1580 (shoulder) and 1540 cm^{-1} ($\nu_{sym}(C-O) + \nu_{asym}(C-C)$), 1424 and 1356 cm^{-1} ($\delta(CH_3)$), 1286 cm^{-1} ($\nu_{sym}(C-C)$), 1026 cm^{-1} ($\rho(CH_3)$), and 938 cm^{-1}.[25] Bands due to acetonitrile and to alkoxy groups are no longer present in the 2300−2200- and 1200−1000-cm^{-1} range, respectively. Wide bands observed between 700 and 500 cm^{-1} were consistent with the formation of Sn−OH and Sn−O−Sn bonds. The broad band centered at 3440 cm^{-1} corresponding to the OH stretching region is in agreement with the presence of water and Sn−OH groups. Consequently, assuming that C atoms belong to acetylacetonato groups, the following formula $SnFO_{1.05}(CH_3COCHCOCH_3)_{0.9}\cdot 0.7H_2O$ can be proposed for xerosol X_2^A. After aging at 60 °C over 3 days, two very broad bands characteristic of amorphous tin oxide were observed on the X-ray diffraction pattern of X_2^A (Figure 3a).

The behavior in solution of xerosols X_2^D, X_{10}^D, and Y_2^A was analogous to that described for X_2^A.[17a] Indeed, solution ^{19}F NMR analyses gave rise to a broadened peak (∼2 ppm) at −77 ppm for Y_2^A and to very broad resonances (∼30 ppm) around −130 ppm for X_2^D and X_{10}^D. These values were consistent with those of fluorine nuclei located on β-diketonate ligands and on the tin center, respectively. Besides, no resonance was detected by ^{119}Sn NMR spectroscopy. This phenomenon has previously been attributed to the formation of large and ill-defined stannic oxopolymeric species.[26]

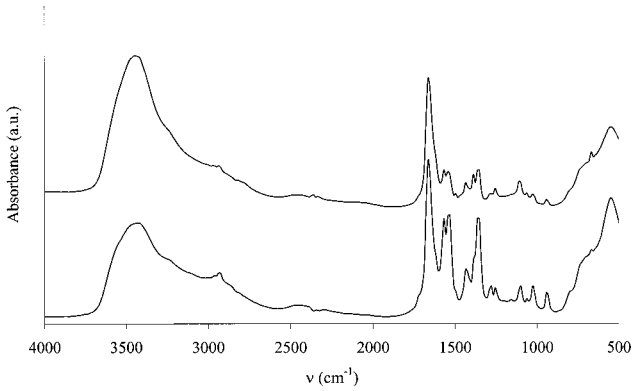

Figure 4. FTIR spectra of xerosols X_2^D (bottom) and X_{10}^D (top) after drying.

In comparison with X_2^A (Figure 2), two main differences were pointed out by IR spectroscopy for xerosols X_2^D and X_{10}^D (Figure 4). The broad bands found in the OH stretching and in the Sn−O−Sn network regions were noticeably more intense when the hydrolysis was led in DMF, and bands at 1662 cm^{-1} (ν(O═C−N)), 1433 cm^{-1} ($\delta(CH_3)$), and 1255 and 1104 cm^{-1} indicate that free or coordinated DMF molecules were trapped in these xerosols. Very wide bands between 800 and 400 cm^{-1} were characteristic of amorphous tin-dioxide-based materials. The band at 540 cm^{-1} is due to the Sn−O stretching vibration of Sn−OH groups.[27] The shoulder around 650 cm^{-1} is consistent with the presence of Sn−O−Sn bonds.[28] Examination of the relative peak intensities showed that both the Sn−O−Sn amount and [DMF]/[$CH_3COCHCOCH_3$] ratio have increased as the hydrolysis ratio was increased. These data were therefore in favor of the formation of more condensed species when, on one hand, *h* was raised and, on the other hand, DMF was used as the solvent. Elemental analysis confirmed these observations, leading to the following formulas: $SnFO_{1.27}(CH_3COCHCOCH_3)_{0.46}(DMF)_{0.37}\cdot 0.7H_2O$ and $SnFO_{1.47}(CH_3COCHCOCH_3)_{0.07}(DMF)_{0.83}\cdot 1.9H_2O$ for X_2^D and X_{10}^D, respectively. X-ray diffraction patterns showed only two wide bands that could be assigned to amorphous tin dioxide (similar to the one shown Figure 3a).

The IR spectrum of Y_2^A was slightly more complicated than that of X_2^A due to the disymmetry of the 1,1,1-trifluoropentan-2,4-dionato ligands, but it did not show any band indicating the presence of an acetonitrile or alcoxy group. Therefore, assuming that C and F atoms belong to β-diketonate groups, the formula $SnO_{1.4}(CF_3COCHCOCH_3)_{1.2}\cdot 0.9H_2O$ can be proposed for xerosol Y_2^A.

(25) Jones, R. W.; Fay, R. C. *Inorg. Chem.* **1973**, *12*, 2599.

(26) Eychenne-Baron, C.; Ribot, F.; Sanchez, C. *J. Organomet. Chem.* **1998**, *567*, 137.

(27) Morrison, J. S.; Haendler, H. M. *J. Inorg. Nucl. Chem.* **1967**, *29*, 393.

(28) Kriegsman, H.; Hoffmann, H. M.; Geissler, H. *Z. Anal. Allg. Chem.* **1965**, *24*, 341.

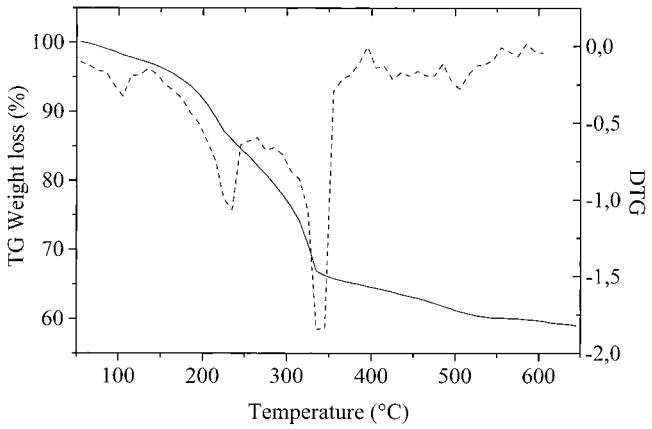

Figure 5. TG and DTG curves of xerosol X_2^A in He.

Table 2. TGA Coupled with MS Data for Xerosol X_2^A

pyrolysis step	sampling temperature (°C)	mass loss intensity %	species detected
I	100	2.9	H_2O, (minor CO_2)
II	219	12.8	CO_2, $(CH_3CO)_2CH_2$, $(CH_3)_2CO$, H_2O
III	325	18.5	F, HF, CO_2, $(CH_3CO)_2CH_2$, $(CH_3)_2CO$, CH_3COOH, H_2O
IV	490	5.3	F, CO_2, (minor HF)

At this stage, whatever the precursor used, hydrolysis and condensation steps have led to a mixture of ill-defined soluble stannic oxo-oligomers or polymers including fluorine and various amounts of β-diketonate ligands. It must also be noted that the F/Sn ratio remained unchanged upon hydrolysis when precursor **1** was used, which shows that the Sn−F bond is stable under the experimental conditions used.

Pyrolysis Experiments. The thermolytic behavior of the xerosols was studied by thermogravimetry coupled to mass spectrometry[29,30] to determine the optimal thermal treatment yielding SnO_2 powder with an amount of doping fluorine and low carbon content.

The TG analysis of X_A^2 shows a continuous mass loss from 50 to 650 °C. Four different stages, 2.9, 12.8, 18.5, and 5.3% mass loss at 100, 219, 325, and 490 °C, respectively, can be distinguished on the DTG curve (Figure 5). The main chemical species (Table 2) released were water (m/z = 17, 18), pentan-2,4-dione (m/z = 99) and its degradation products (m/z = 60: acetic acid; m/z = 58: acetone; m/z = 43: acetyl), and fluorine (m/z = 20: fluorhydric acid; m/z = 19: fluorine) as depicted in Figure 6. No significant amount of acetonitrile (m/z = 41) was detected.

The first weight loss at 100 °C can be assigned to the release of adsorbed or trapped water in the xerosol.[31] A second contribution of the release of water, maximum at 325 °C as evidenced from the trend of the 17 and 18 m/z ions versus temperature, comes from the condensation of two Sn−OH moieties with the formation of oxo-bridges Sn−O−Sn and structural water removal. These oxolation reactions are activated by different parameters such as thermally induced network contraction

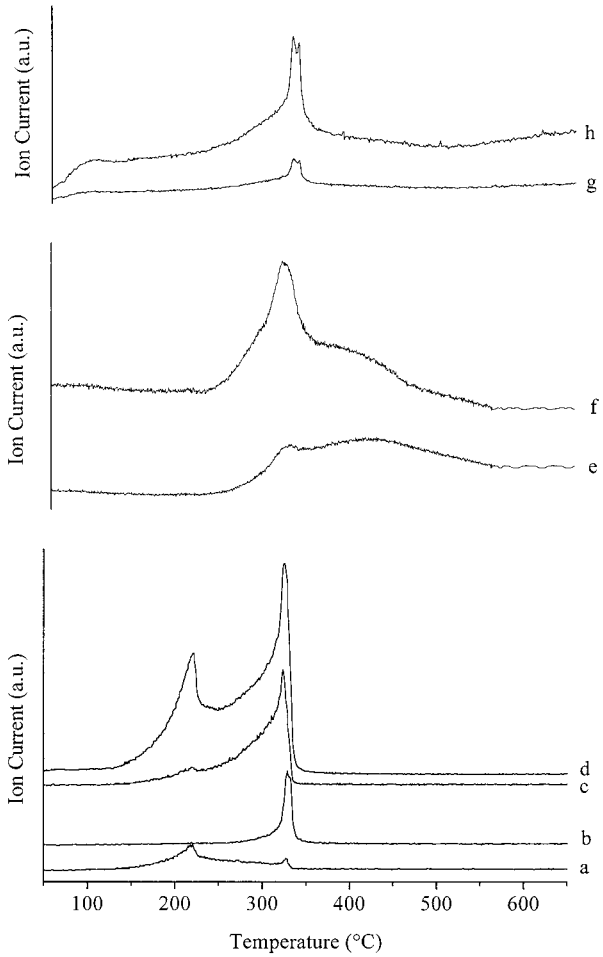

Figure 6. Xerosol X_2^A m/z curves as a function of temperature. (a) $CH_3COCHCOCH_3$; (b) CH_3COOH; (c) CH_3COCH_3; (d) CH_3CO; (e) F; (f) HF; (g) OH; (h) H_2O.

and the sterical hindrance decrease around the tin atom generated by the pyrolysis of the organic products during steps II and III (Table 2).[31]

Departure of pentan-2,4-dionato ligands takes place between 150 and 350 °C with two maxima at 219 and 325 °C as indicated by the profile of the 99 m/z ion. These steps may be rationalized by postulating the hydrolysis of the ligands due to structural water:

$$\equiv Sn-O-\underset{\displaystyle CH_3}{\overset{\displaystyle |}{C}}-CH-CO-CH_3\,(s) \xrightarrow{H_2O} \equiv Sn-OH\,(s) + CH_3COCH_2COCH_3 \quad (2)$$

The pentan-2,4-dione detection is accompanied by acetyl, acetone, and acetic acid fragments.[18,30,32] Acetone is detected during stages II and III with a maximum at 325 °C correlated to the second maximum observed in the 99 m/z profile characteristic of pentan-2,4-dione. In contrast to the results described on acetylacetone-modified zirconium oxide gels,[30] the main acetone release occurs before the detection of acetic acid. Below 300 °C, the formation of acetone must therefore be assigned to a concerted reaction involving two close

(29) (a) Belot, V.; Corriu, R. J. P.; Leclercq, D.; Mutin, P. H.; Vioux, A. *J. Mater. Sci. Lett.* **1990**, *9*, 1052. (b) Bouillon, E.; Langlais, F.; Pailler, R.; Naslain, R.; Cruege, F.; Huong, P. V.; Sarthou, J. C.; Delpuech, A.; Laffon, C.; Lagarde, P.; Monthioux, M.; Oberlin, A. *J. Mater. Sci.* **1991**, *26*, 1333.

(30) Di Maggio, R.; Campostrini, R.; Guella, G. *Chem. Mater.* **1998**, *10*, 3839.

(31) Pierre, A. C. *Introduction to Sol−Gel Processing*; Kluwer: Boston, 1998.

(32) Scolan, E.; Sanchez, C. *Chem. Mater.* **1998**, *10*, 3217.

pentan-2,4-dionato ligands and structural water as proposed by Di Maggio et al.:[30]

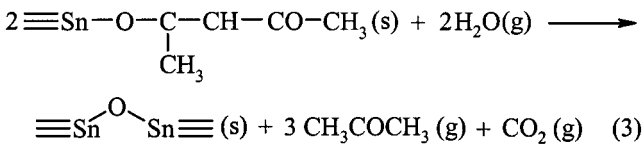

This process was assessed by the detection of $CO_2^{\bullet+}$ fragment both in stages II and III. In contrast, acetic acid and acetone were found above 300 °C, which is in favor of a thermal decomposition of the chelating groups via retro-Claisen reactions catalyzed by the presence of Lewis acids such as tin(IV) or traces of water in the xerosol:[33]

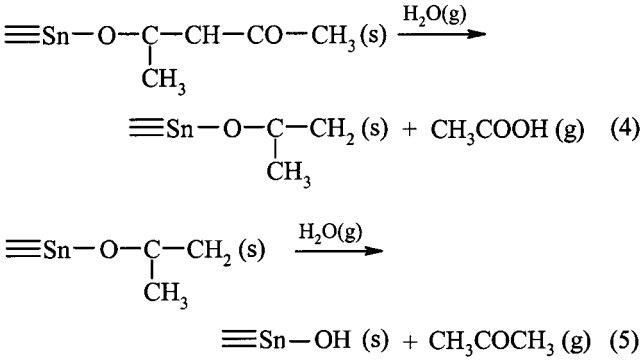

This process induces the formation of Sn−OH groups, leading to water release via oxolation reactions, which explains the second maximum (325 °C) observed on the water profile.

Fluorine loss mainly occurs as fluorhydric acid and starts from 230 °C, concomitantly with structural water departure, with two maxima, a major at 325 °C and a minor around 430 °C. The HF formation is probably due to the Sn−F bond cleavage in the presence of traces of water, giving rise to new Sn−OH that form water again. It is therefore a catalytic process. In addition, the $F^{\bullet+}$ fragment is continuously detected between 300 and 560 °C with a maximum around 430 °C, after the elimination of the main organic products. The mass loss above 350 °C seems to be due to the loss of fluorine and to the formation of CO_2 from residual carbon.

Interpretation of TGA/MS measurements carried out on xerosols X_2^D and X_{10}^D was more intricate due to the presence of a rather large amount of DMF in the xerosols. It was indeed continuously released between 100 and 320 °C as evidenced by the 73 *m*/*z* ion versus temperature profile and also contributed to both 43 and 58 *m*/*z* peaks, previously assigned to acetyl and acetone fragments, respectively.[34] The TG-DTG analysis of X_2^D displayed a large mass loss consisting of two significant stages at 310 °C (25% mass loss) and around 520 °C (~5% mass loss). The main chemical species evolved during the thermolysis were water, fluorhydric acid, acetic acid, DMF, and pentan-2,4-dione, while the formation of acetone cannot unambiguously be asserted for the reason underlined above. The evolutions of water and fluorine species were quite similar to those described for X_2^A. In contrast, a single acetylacetone loss took place at 310 °C just followed by the acetic acid release, which accounts for a predominant retro-Claisen-type degradation process of the chelating ligands. In the case of X_{10}^D, neither pentan-2,4-dione nor acetic acid could be detected. This is in agreement with the low acetylacetone amount deduced from elemental analysis and IR spectroscopy measurements. The thermogravimetric curve can be rationalized in terms of successive departures of adsorbed and structural water, DMF, and fluorine.

The shape of the TG−DTG curve recorded for xerosol Y_2^A was roughly similar to that of X_2^A. Four mass losses were observed on TG traces and the main molecules detected by MS measurements were H_2O, HF, 1,1,1-trifluoropentan-2,4-dione, acetone, acetic acid, and species characterized by $CF_3CO^{\cdot+}$ fragments such as trifluoroacetic acid or trifluoroacetone.[34] The different pyrolysis stages should be interpreted as follows: (1) elimination of adsorbed water and acetone (100 °C, 3.7% mass loss); (2) first step of the 1,1,1-trifluoropentan-2,4-dione release (200 °C, 6.8% mass loss); (3) loss of structural water, part of fluorine and second step of the 1,1,1-trifluoropentan-2,4-dione elimination with the corresponding degradation products (337 °C, 37.4% mass loss); (4) subsequent loss of fluorine and remaining carbon as CO_2 (530 °C, 13.4% mass loss). The fluorine loss was revealed by the detection of the $CF_3CO^{\bullet+}$ and $CF_3^{\bullet+}$ ion fragments, but also by $HF^{\bullet+}$ and $F^{\bullet+}$ fragments exhibiting temperature profiles near those observed for the other xerosols. Consequently, the formation of fluorhydric acid could be at the origin of the fluorine insertion in the tin dioxide network, improving the conductivity properties. This will be confirmed in the following.

To summarize, the TGA/MS analyses assess the nature of the organics present after hydrolysis and show that most of the fluorine and the organics were removed after thermal treatment above 500 °C.

Characterization of the Thermolyzed Xerosols. Preliminary studies carried out on X_2^A demonstrated that both temperature and time of the thermal treatment ruled the crystallinity and the chemical composition of the resulting sol−gel tin dioxide materials.[17a,b] According to these findings, the different xerosols were calcined in air at 550 °C for 30 min, a thermal treatment allowing crystallization of tin dioxide.[17a] All the obtained materials exhibited a similar X-ray diffraction pattern and close IR and Mössbauer spectra. The IR spectrum accounts for the complete removal of the chelating ligands and mainly shows a broad peak centered at 625 cm^{-1} assigned to the Sn−O−Sn network.[22] Besides, the isomeric shift (δ = 0.01 mm s^{-1}) inferred from Mössbauer measurements (Figure 1B) and the shape of the XRD pattern (Figure 3b) are consistent with the formation of crystalline particles of SnO_2 cassiterite,[35] the particle size was estimated to be 7−8 nm (Table 3). Nanocrystalline sol−gel materials were therefore prepared.

(33) Poncelet, O.; Hubert-Pflalzgrah, L. G. *Polyhedron* **1990**, *9*, 1305.

(34) See Supporting Information.

(35) *Powder Diffraction File*; JCPDS International Center for Diffraction Data: Swarthmore, PA, 1998; no. 41-1445.

Table 3. Chemical Composition, Resistivity (ρ), and Crystallite Size (t) of the Different Materials Prepared after Thermal Treament in Air at 550 °C for 30 min

xerosol	F/Sn atom	C/Sn atom	ρ (Ω.cm)	t (nm)
X_2^A	0.06	0.12	0.8	8
X_2^D, X_{10}^D	0.08	0.16	2	7
Y_2^A	0.04	0.09	17	7
Z_2^A		0.11	10^3	8
SnO_2 (Aldrich)			2×10^3	50

Their resistivities measured under pressure are gathered in Table 3. It must be underlined that only a comparison of the resistivity of samples measured using similar experimental conditions is meaningful because an unnegligible drop of the carrier mobility is induced by the powder nature of the studied samples. The results were therefore compared to those obtained with undoped SnO_2 powders prepared from commercial starting materials. As expected, samples containing fluorine showed resistivities several orders of magnitude lower than that of undoped SnO_2. The thermolyzed xerosol X_2^A exhibited resistivity as low as 0.8 Ω cm, 1 order of magnitude lower than that reported for Sb-doped SnO_2 powders.[6b] For this material, an atomic ratio of F/Sn = 0.06 was found by elemental analysis, which is in the range of the best doping rate of tin dioxide materials.[36] Another striking feature is the low resistivity found despite the nanocrystalline character of the X_2^A-derived material. This indicates the high conductivity of each elementary grain of the sol−gel sample, compared to that of the reference material that exhibits crystallite size nearly 1 order of magnitude larger.

Xerosols prepared in DMF led to nanocrystalline powders showing twice as high resistivities, probably due to larger carbon contents. Besides, a doping of tin dioxide by fluorine took place in the Y_2^A-derived material as evidenced by elemental analysis and resistivity measurements. Fluorine probably moved from $-CF_3$ groups of the chelating ligands toward tin atoms either after the fluorhydric acid formation occurring during the combustion of the organics or after the decomposition of the fluorinated ligands into metal fluorides via concerted elimination reactions.[37,10a,c,d] However, the resulting material was 1 order of magnitude more resistive than the previous one. Consequently, the best strategy to incorporate doping fluorine into tin dioxide sol−gel materials seems to be through the pre-existence of an Sn−F bond in the precursor.

In the case of the xerosols X and Y, carbon removal was attempted by increasing the time of the thermal treatment. A concomitant decrease of both carbon and fluorine contents was observed, leading to a conductivity drop. At this stage, one has to emphasize that the duration of the thermal treatment at a given temperature allowed one to control the fluorine amount in the final material. Whatever the fluorinated xerosol studied, the optimal time at 550 °C was 30 min.

On the basis of the previous findings, the origin of the low resistivity found for X_2^A is questionable. The electrical properties of F-doped tin dioxide is usually explained as follows. In the presence of fluorine, tin dioxide becomes a degenerated semiconductor and the mechanism of formation of electronic carriers could be

$$xF^- + xe^- + Sn^{4+}O_2^{2-} \rightleftharpoons Sn^{4+}O_{(2-x)}^{2-}F_x^-[xe^-]_{C.B.} + xO^{2-}$$

where $[xe-]_{C.B.}$ represents the concentration in electrons generated in the conduction band and responsible for the conduction.

In the absence of the other electron source, the concentration in charge carriers is at the most the concentration of the doping element introduced in the oxide network. Besides, the formation of defects, such as oxygen vacancies, also release electrons in the conduction bands:

$$Sn^{4+}O_2^{2-} \rightleftharpoons Sn^{4+}O_{(2-\delta)}^{2-}\square_\delta[2\delta e^-]_{C.B.} + {}^1/_2\delta O_2$$

These two mechanisms can coexist. However, the high resistivity found both with SnO_2 (Aldrich) and thermolyzed xerosol Z_2^A shows that this second mechanism does not prevail. In addition, the carbon content observed in the latter was similar to that found in the other sol−gel samples, showing that carbon did not significantly participate in the conduction. Consequently, the low resistivities measured are mainly related to the incorporation of fluorine in the tin oxide network. For the X_2^A sample, this incorporation would occur in such a way that the corresponding electron-donor centers are located at the immediate vicinity of the conduction band, so that they can generate highly mobile electron, leading to the observed low resistivity.

Concluding Remarks

Hydrolysis and condensation of fluorinated β-diketonate tin(IV) complexes **1** and **2** gave soluble stannic oxo-oligomeric or polymeric species including fluorine and various amounts of chelating ligands. In these reactions, (1) the Sn−F bond remains unaffected under the conditions used, (2) the β-diketonate groups are more easily removed in a polar aprotic and coordinating solvent such as DMF, and (3) a large amount of DMF is trapped in the resulting materials.

TG/MS measurements showed that during the thermolysis step of the xerosols (1) the β-diketonate ligands pyrolyze in two stages at 200 and 320 °C involving two different processes and (2) elimination of a very polar solvent exhibiting a high boiling point, such as DMF, occurs up to 300 °C, which diminishes the interest to use such a solvent to remove most of the β-diketonate ligands; (3) fluorine is lost as fluorhydric acid from 230 °C. In this respect, this study contributes to the elucidation of the fluorine removal, which is passed over in silence in most studies dealing with the development of F-doped tin dioxide materials. In particular, this explains why a large amount in the fluorine source is necessary in solution used for thin film preparation by "spray" pyrolysis.[38]

(36) The best doping amount is between 1 and 8 at. %F per Sn atom. See ref 10b and also see Fantini, M.; Torriani, I. *Thin Solid Films* **1986**, *138*, 255.

(37) Samuels, J. A.; Chiang, W.-C.; Yu, C. P.; Apen, E.; Smith, D. C.; Baxter, D. V.; Caulton, K. G. *Chem. Mater.* **1994**, *6*, 1684.

(38) Acosta, D. R.; Zironi, E. P.; Montoya, E.; Estrada, W. *Thin Solid Films* **1996**, *288*, 1.

The samples thermally treated in air at 550 °C yield nanocrystalline tin dioxide powders containing a doping amount of fluorine with resistivities lower than those described for Sb-doped tin dioxide powders. Our results indicate that the best strategy to prepare F-doped SnO_2 materials by the sol−gel route is to start from precursors including Sn−F bonds and to use a polar aprotic solvent of low boiling point.

We are currently exploring the use of these soluble materials for thin film preparation[39] and the feasibility and the merits of the thermolyzed xerosols in lithium insertion batteries.[40]

Acknowledgment. Dr. L. Fournès and Dr. L. Rabardel are acknowledged for Mössbauer studies and TGA/MS measurements, respectively. Bernard Barbe, Michel Petraud, and Christophe Soumaille are thanked for their precious assistance.

Supporting Information Available: Synthesis and characterization of bis(*tert*-amyloxy)di(1,1,1-trifluoropentan-2,4-dionato)tin(IV) **2** and thermogravimetry coupled to mass spectrometry analyses of xerosols X_2^D, X_{10}^D, and Y_2^A). This material is available free of charge via the Internet at http://pubs.acs.org.

CM001073K

(39) Cachet, H.; Gamard, A.; Campet, G.; Jousseaume, B.; Toupance, T. *Thin Solid Films*, submitted.

(40) Brousse, T.; Retoux, R.; Herterich, U.; Schleich, D. M. *J. Electrochem. Soc.* **1998**, *145*, 1.